at high angles of attack. Moreover, the improvements in the lift coefficient for the combination of the two apex flaps were more effective than for the single flap.

Acknowledgment

The project was supported by the Aeronautic Science Foundation of China.

References

[1]Wood, N. J., and Roberts, L., "The Control of Vortical Lift on Delta Wings by Tangential Leading-Edge Blowing," AIAA Paper 87-0158, Jan. 1987.

[2]Gu, W., Robinson, O., and Rockwell, D., "Control of Vortices on a Delta Wing by Leading-Edge Injection," *AIAA Journal*, Vol. 31, No. 7, 1993, pp. 1177–1186.

[3]Rinoie, K., and Stollery, J. L., "Experimental Studies of Vortex Flaps and Vortex Plates," *Journal of Aircraft*, Vol. 31, No. 2, 1994, pp. 322–329.

[4]Srigrarom, S., and Kurosaka, M., "Shaping of Delta-Wing Planform to Suppress Vortex Breakdown," *AIAA Journal*, Vol. 38, No. 1, 2000, pp. 183–186.

[5]Helin, H. E., and Watry, C. W., "Effects of Trailing-Edge Jet Entrainment on Delta Wing Vortices," *AIAA Journal*, Vol. 34, No. 7, 1996, pp. 802–804.

[6]Rao, D. M., and Buter, T. A., "Experimental and Computational Studies of a Delta Wing Apex Flap," AIAA Paper 83-1815, July 1983.

[7]Lowson, M. V., and Riley, A. J., "Vortex Breakdown Control by Delta Wing Geometry," *Journal of Aircraft*, Vol. 32, No. 4, 1995, pp. 832–838.

[8]Klute, S. M., Rediniotis, O. K., and Telionis, D. P., "Flow Control over a Maneuvering Delta Wing at High Angles of Attack," *AIAA Journal*, Vol. 34, No. 4, 1996, pp. 662–668.

[9]Lambourne, N. C., and Bryer, D. W., "The Bursting of Leading Edge Vortices—Some Observations and Discussion of the Phenomenon," Aeronautical Research Council, Repts. and Memoranda, No. 3282, 1961, pp. 1–37.

A. Plotkin
Associate Editor

Three-Dimensional Benchmark Problem for Broadband Time-Domain Impedance Boundary Conditions

Shi Zheng* and Mei Zhuang†
Michigan State University, East Lansing, Michigan 48824

Introduction

AEROACOUSTIC problems in liner technology are an important category of the application of computational aeroacoustics (CAA). Because of the limitations of the frequency-domain simulations, the time-domain impedance boundary conditions in CAA applications have been exploited in the past few years. Because liner impedance is conventionally defined in frequency domain, it is desirable to convert characteristics of impedance in the frequency domain into the time domain so that the information can serve as a well-posed boundary condition for the linearized Euler equations. Several approaches of converting the frequency-domain impedance boundary condition into the time domain have been carried out,[1–4] one of which was developed by Tam and Auriault.[1] They have proved the well-posednature and stability of their impedance boundary conditions, but have not tested their boundary conditions in a dimensionality higher than one. In this Note, a three-dimensional acoustic problem with an impedance boundary is proposed. The analytical solution is derived and then is used to test the numerical solution due to such a time-domain impedance boundary condition.

Received 3 August 2002; revision received 5 June 2003; accepted for publication 20 July 2003.

*Graduate Research Assistant, Department of Mechanical Engineering.
†Associate Professor, Department of Mechanical Engineering. Senior Member AIAA.

Test Problem Formulation

The test problem is shown in Fig. 1. The domain of interest lies in the ranges of $-\infty < x < \infty$, $-\infty < y < \infty$, and $z \geq 0$. A liner with uniform impedance $Z(\omega) = \hat{p}(\omega)/\hat{v}_n(\omega)$ is applied at $z = 0$, where $\hat{p}$ and $\hat{v}_n$ are acoustic pressure and particle velocity $\hat{v}_n$ normal to the liner (positive when pointing into the liner) in the frequency domain. A spherical Gaussian acoustic pressure pulse $p_0(R) = \exp(-BR^2)$ is initially introduced with zero initial velocity components, where constant $B > 0$ and R is the distance to the pulse center at $S(0, 0, z_S)$. Note that all of the quantities in this Note are nondimensionalized such that the speed of sound is unity.

Analytical Solution

The analytical solution of the test problem is considered to be the superposition of three component waves, that is, the outgoing wave, which diverges from the sphere center; the incoming wave, which converges to the sphere center; and the reflected wave by the impedance boundary. A broadband incident wave needs to be decomposed into harmonic waves, and a nonplane incident wave needs to be decomposed into plane waves. Then the reflection of each of the harmonic plane incident waves by the impedance boundary can be determined. The total reflected wave is in a form of an integral of the reflected harmonic plane waves. This is the general idea for deriving the analytical solution to our test problem.

The outgoing and incoming waves in free space with the same initial condition can be determined, in terms of the velocity potential φ defined by $\nabla\varphi = \boldsymbol{v}$ with spherical symmetry,[5] to be

$$\varphi_{\text{out}}(R, t) = f(R - t)/R \tag{1}$$

$$\varphi_{\text{in}}(R, t) = -f(R + t)/R \tag{2}$$

where $R = \sqrt{[x^2 + y^2 + (z - z_s)^2]}$ and f is determined from the initial condition to be $f(r) = -\exp(-Br^2)/(4B)$, for $-\infty < r < \infty$.

For the test problem, the outgoing and incoming waves are not exactly the same as the given free space solutions. This is because the actual initial condition is not a complete spherical Gaussian pulse, part of which is outside the semi-infinite space. However, if the center of the spherical pulse is far away from the impedance boundary, the outside portion of the initial pulse will be of very small amplitude and, thus, insignificant to the whole problem. Therefore, we can safely assume a complete initial spherical Gaussian pulse for the test problem and approximate its outgoing and incoming waves with the free space solution in Eqs. (1) and (2). Such treatment will greatly simplify the analysis. The reflected wave is determined by considering the incident (outgoing) wave φ_{out} in Eq. (1) being reflected by the impedance boundary. As stated earlier, the broadband spherical outgoing wave must be decomposed into harmonic plane components to study the effects of the impedance boundary. This decomposition process is done in the following two steps, which can be done in reverse order:

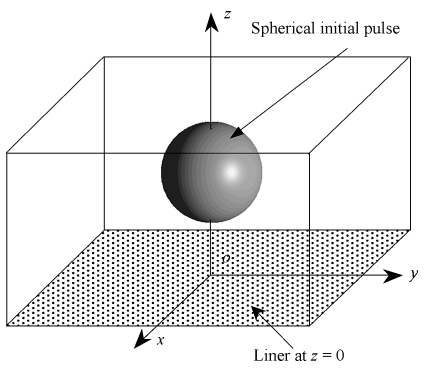

Fig. 1 Schematic of the test problem.

In the first step, the broadband outgoing spherical wave φ_{out} is decomposed into harmonic outgoing spherical waves

$$\varphi_{\text{out}}(R,t)=\int_{-\infty}^{\infty}\hat{f}(k_0)\frac{\exp[ik_0(R-t)]}{R}\,\mathrm{d}k_0 \tag{3}$$

by resolving function $f(R-t)$ into its Fourier transform $\hat{f}(k_0)=\exp[-k_0^2/(4B)]/[8B\sqrt{(\pi B)}]$, which is real and even because $f(R-t)$ is real, even, and summable.[6] Obviously the expression $\exp[ik_0(R-t)]/R$ in the integrand of Eq. (3) represents a harmonic outgoing spherical wave with an angular frequency/wave number k_0. (The speed of sound is unity.) Because $\hat{f}(k_0)$ is real and even, the integration in Eq. (3) can be performed only over the nonnegative range of angular frequency/wave number k_0 with the real part of the integral unchanged:

$$\varphi_{\text{out}}(R,t)=2\mathrm{Re}\left\{\int_0^{\infty}\hat{f}(k_0)\frac{\exp(-ik_0t)\exp(ik_0R)}{R}\,\mathrm{d}k_0\right\} \tag{4}$$

For the sake of convenience, the time dependence is separated from the harmonic spherical wave, which will then be represented only by the term $\exp(ik_0R)/R$ in the following derivation.

As the second step of the decomposition process, a harmonic spherical wave $\exp(ik_0R)/R$ with a nonnegative angular frequency/wave number k_0 is decomposed into harmonic plane waves, using Weyl's integral (see Refs. 7 and 8):

$$\frac{\exp(ik_0R)}{R}=\frac{i}{2\pi}\int_{-\infty}^{\infty}\int_{-\infty}^{\infty}\exp\{i[k_xx+k_yy+k_z(z-z_S)]\}\frac{\mathrm{d}k_x\mathrm{d}k_y}{k_z}$$

$$\text{for}\quad z>0 \tag{5}$$

where $\exp\{i[k_xx+k_yy+k_z(z-z_S)]\}$ represents a harmonic plane wave with $k_z=\sqrt{(k_0^2-k_x^2-k_y^2)}$.

By now, the broadband spherical incident wave has been decomposed into harmonic plane waves, and thus, it is ready to incorporate the effects of the impedance boundary on each of these harmonic plane incident waves. When the method of mirror image is used, the reflected wave of each of the harmonic plane waves in the integrand of Eq. (5) by the impedance boundary is determined to be

$$C_r(k_0,k_z)\exp\{i[k_xx+k_yy+k_z(z+z_S)]\} \tag{6}$$

where the reflection coefficient $C_r(k_0,k_z)$ is determined from the liner impedance $Z(\omega)$:

$$C_r(k_0,k_z)=\frac{[Z(k_0)(k_z/k_0)-1]}{[Z(k_0)(k_z/k_0)+1]} \tag{7}$$

Corresponding to Eq. (5), the reflected harmonic (nonplane) outgoing wave is then obtained by integrating the reflected harmonic plane waves in Eq. (6):

$$\varphi_{k_0,\text{refl}}(x,y,z,k_0)=\frac{i}{2\pi}\int_{-\infty}^{\infty}\int_{-\infty}^{\infty}C_r(k_0,k_z)$$

$$\times\exp\{i[k_xx+k_yy+k_z(z+z_S)]\}\frac{\mathrm{d}k_x\mathrm{d}k_y}{k_z} \tag{8}$$

Similarly, the reflected wave of the outgoing wave in Eq. (4) is obtained by integrating the reflected harmonic (nonplane) wave in Eq. (8):

$$\varphi_{\text{refl}}(x,y,z,t)=2\mathrm{Re}\left\{\int_0^{\infty}\hat{f}(k_0)\exp(-ik_0t)\varphi_{k_0,\text{refl}}(R,k_0)\,\mathrm{d}k_0\right\} \tag{9}$$

By changing the variables of integration and separating the real and the imaginary parts of Eq. (8), we have

$$\mathrm{Re}[\varphi_{k_0,\text{refl}}(x,y,z,k_0)]$$

$$=k_0\int_{-1}^{0}C_1\sin(k_0z'\xi-\beta_1)J_0\left[k_0r\sqrt{1-\xi^2}\right]\mathrm{d}\xi$$

$$+k_0\int_0^{\infty}C_2\cos(\beta_2)\exp(-k_0z'\xi)J_0\left[k_0r\sqrt{1+\xi^2}\right]\mathrm{d}\xi$$

$$\mathrm{Im}[\varphi_{k_0,\text{refl}}(x,y,z,k_0)]$$

$$=k_0\int_{-1}^{0}C_1\cos(k_0z'\xi-\beta_1)J_0\left[k_0r\sqrt{1-\xi^2}\right]\mathrm{d}\xi$$

$$+k_0\int_0^{\infty}C_2\sin(\beta_2)\exp(-k_0z'\xi)J_0\left[k_0r\sqrt{1+\xi^2}\right]\mathrm{d}\xi$$

where J_0 is the Bessel function of the first kind of order zero and C_1, C_2, β_1, and β_2 are the moduli and arguments of reflection coefficients $C_r(k_0,-k_0\xi)$ and $C_r(k_0,ik_0\xi)$ defined in Eq. (7),

$$C_1=|C_r(k_0,-k_0\xi)|,\qquad \beta_1=\arg[C_r(k_0,-k_0\xi)]$$

$$C_2=|C_r(k_0,ik_0\xi)|,\qquad \beta_2=\arg[C_r(k_0,ik_0\xi)]$$

When the derivatives of the velocity potential, are taken, the acoustic pressure and the components of the particle velocity can be determined. Specially, the acoustic pressures associated with the outgoing, incoming and reflected waves are determined from Eqs. (1), (2) and (9):

$$p_{\text{out}}(x,y,z,t)=-\frac{\partial}{\partial t}\varphi_{\text{out}}(R,t)=\frac{R-t}{2R}\exp[-B(R-t)^2] \tag{10}$$

$$p_{\text{in}}(x,y,z,t)=-\frac{\partial}{\partial t}\varphi_{\text{in}}(R,t)=\frac{R+t}{2R}\exp[-B(R+t)^2] \tag{11}$$

$$p_{\text{refl}}(x,y,z,t)=-\frac{\partial}{\partial t}\varphi_{\text{refl}}(x,y,z,t)$$

$$=2\int_0^{\infty}k_0\hat{f}(k_0)[\sin(k_0t)\mathrm{Re}(\varphi_{k_0,\text{refl}})$$

$$-\cos(k_0t)\mathrm{Im}(\varphi_{k_0,\text{refl}})]\,\mathrm{d}k_0 \tag{12}$$

which has to be evaluated using numerical integration. The total acoustic pressure is given by the sum of Eqs. (10–12).

Numerical Implementation

Broadband Dispersion-Relation-Preserving Upwind Scheme

A fourth-order seven-point-stencil optimized upwind dispersion-relation-preserving (DRP) scheme with the parameters[9] chosen as $\beta_0=\pi/2$, $\lambda=0.0374$, and $\sigma=0.2675\pi$ is used for the numerical simulation of the Euler equations. The approximation coefficients used in the scheme for the interior and boundary points are the same as those listed in Ref. 9.

Broadband Time-Domain Impedance Boundary Condition

For the impedance of the Helmholtz resonator type characterized by

$$Z(\omega)=R_0-i(X_{-1}/\omega+X_1\omega) \tag{13}$$

where R_0, X_{-1}, and X_1 are constant parameters, and the broadband time domain impedance boundary condition is given by Tam and Auriault[1] as

$$\frac{\partial p}{\partial t}=R_0\frac{\partial v_n}{\partial t}-X_{-1}v_n+X_1\frac{\partial^2 v_n}{\partial t^2} \tag{14}$$

where p and v_n are the acoustic pressure and the normal acoustic velocity at the impedance boundary (positive when pointing into the liner) in the time domain. Because in a discrete form both the Euler equations and the impedance boundary condition (14) have to

be satisfied on the nodes at the impedance boundary, extra freedom must be introduced to accommodate this requirement. For this purpose, a ghost value for pressure is introduced on a point outside the computational domain one grid spacing away from each of those boundary nodes. For the test problem, the discretized ghost value for pressure at time level n is

$$p^{(n)}_{i,j,\text{ghost}} = \left\{ \Delta z s_{i,j} - \sum_{l=0}^{5} a_l^{15} p_{i,j,l} \right\}^{(n)} \Big/ a_{-1}^{15} \tag{15}$$

where

$$s^{(n+1)}_{i,j} = s^{(n)}_{j,k} + \Delta t \sum_{l=0}^{3} b_l \left\{ -\left[\left(\frac{\partial u}{\partial x} + \frac{\partial v}{\partial y} + \frac{\partial w}{\partial z} \right)_{i,j,0} + R_0 s_{i,j} + X_{-1} w_{i,j,0} \right] \Big/ X_1 \right\}^{(n-l)}$$

and a_l^{15} and b_l are the coefficients for spatial and temporal discretization of the DRP scheme.

Nonreflecting Radiation Boundary Condition

The boundary conditions at all of the boundaries other than the impedance boundary should be able to simulate the situation of a semi-infinite space by allowing the waves to leave the finite computational domain without being reflected. This physical condition is approximated by the nonreflecting radiation boundary conditions for the three-dimensional case

$$\left(\frac{\partial}{\partial t} + \frac{\partial}{\partial r} + \frac{1}{r} \right) [\rho, \boldsymbol{v}^T, p]^T = 0 \tag{16}$$

where r is the distance between the current boundary point and a fixed point inside the computational domain.

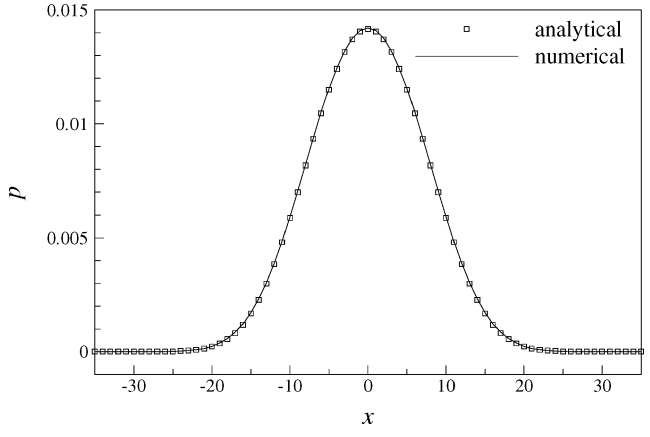

a)

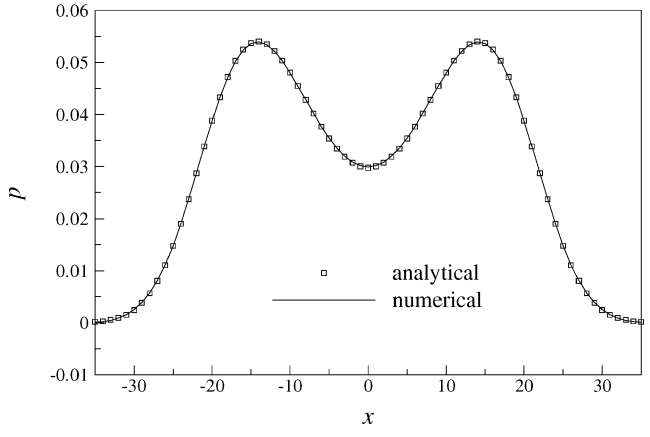

b)

Fig. 2 Comparison of the acoustic pressure along the x axis at a) $t = 20$ and b) $t = 30$.

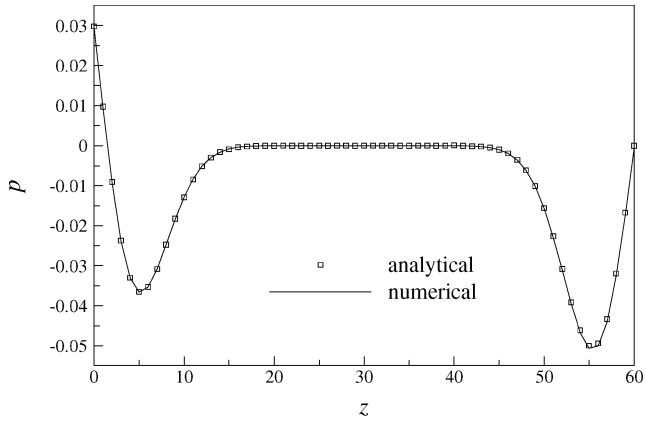

Fig. 3 Comparison of the acoustic pressure along the z axis at $t = 30$.

Comparison of the Results

In the test problem, the initial acoustic pressure pulse $p_0(R) = \exp(-BR^2)$ with $B = (\ell_n 2)/25$ is centered at $S(0, 0, 30)$. The three parameters for the impedance model are $R_0 = 0.2$, $X_{-1} = -0.4758$, and $X_1 = 2.0938$.

The results from the numerical simulation are compared with the analytical solution for the test problem. The acoustic pressure along the x axis, which is at the impedance boundary, at $t = 20$ and $t = 30$ is shown in Figs. 2a and 2b. Shown in Fig. 3 is the acoustic pressure along the z axis at $t = 30$. The asymmetry about $z = 30$, where the center of the initial spherical pulse lies, shows the effect of the impedance boundary. As we can see in Figs. 2 and 3, the numerical solutions agree very well with the analytical solutions, and thus, the time-domain broadband impedance boundary condition is verified.

Conclusions

The analytical solution of a three-dimensional initial and impedance boundary problem is derived and evaluated. The proposed problem can be used to benchmark broadband time-domain impedance boundary conditions in a three-dimensional context. The numerical solution using Tam and Auriault's[1] broadband time-domain impedance boundary condition very accurately reproduces the analytical solution. The excellent agreement gives us confidence in both the benchmark problem and the impedance boundary condition.

References

[1]Tam, C. K. W., and Auriault, L., "Time-Domain Impedance Boundary Conditions for Computational Aeroacoustics," *AIAA Journal*, Vol. 34, No. 5, 1996, pp. 917–923.

[2]Özyörük, Y., and Long, L. N., "A Time-Domain Implementation of Surface Acoustic Impedance Condition with and Without Flow," *Journal of Computational Acoustics*, Vol. 5, 1997, pp. 277–296.

[3]Özyörük, Y., Long, L. N., and Jones, M. G., "Time-Domain Numerical Simulation of a Flow-Impedance Tube," *Journal of Computational Physics*, Vol. 146, 1998, pp. 29–57.

[4]Fung, K.-Y., and Ju, H., "Impedance and Its Time-Domain Extensions," *AIAA Journal*, Vol. 38, No. 1, 2000, pp. 30–38.

[5]Whitham, G. B., *Linear and Nonlinear Waves*, Wiley, New York, 1974, pp. 215–218.

[6]Arsac, J., *Fourier Transforms and the Theory of Distributions*, Prentice–Hall, Englewood Cliffs, NJ, 1966, pp. 35–38.

[7]Poritsky, H., "Extension of Weyl's Integral for Harmonic Spherical Waves to Arbitrary Wave Shapes," *Communications on Pure and Applied Mathematics*, Vol. 4, 1951, pp. 33–42.

[8]Roseau, M., *Asymptotic Wave Theory*, North-Holland, Amsterdam, 1976, pp. 84–86.

[9]Zhuang, M., and Chen, R. F., "Applications of High-Order Optimized Upwind Schemes for Computational Aeroacoustics," *AIAA Journal*, Vol. 40, No. 3, 2002, pp. 443–449.

H. M. Atassi
Associate Editor